Available online at www.sciencedirect.com
SCIENCE DIRECT®
Journal of Nuclear Materials 353 (2006) 1–11
journal of nuclear materials
www.elsevier.com/locate/jnucmat

A model of chemistry and thermal hydraulics in PWR fuel crud deposits

Jim Henshaw [a,*], John C. McGurk [a], Howard E. Sims [a], Ann Tuson [b], Shirley Dickinson [b], Jeff Deshon [c]

[a] *Nexiasolutions (BNFL), Building 168, Harwell, Didcot, Oxfordshire, OX11 0QJ, UK*
[b] *AEA Technology, B44, Winfrith Technology Centre, Dorchester, Dorset, DT2 8WQ, UK*
[c] *Electric Power Research Institute (EPRI), 3412 Hillview Ave., Palo Alto, CA 94304-1395, USA*

Received 4 January 2005; accepted 31 January 2005

Abstract

A model is described for simulating thermal hydraulic and chemical conditions within fuel crud deposits. Heat transfer takes place by wick boiling in which water flows through the porous deposit and evaporates into steam at the surface of chimneys. The transport and chemistry of dissolved species within the deposit is also modelled. This chemistry includes the equilibrium chemistry of Li/boric acid species, the equilibrium chemistry of Fe/Ni species and the radiolysis chemistry of water. The unique feature of this model is that the chemistry is coupled to the thermal hydraulics via the increase in the saturation temperature with the concentration of dissolved species. This has a profound effect on evaporative heat transfer within thick deposits, leading to conditions that explain the precipitation of $LiBO_2$ and the possible formation of bonaccordite. The model helps understand several crud scrape observations, including why AOA is observed to occur for a crud thickness in the region of 20–30 μm.

1. Introduction

The axial offset (AO) of a PWR plant is the integrated power output in the top half of the core minus the integrated power over the bottom half, all divided by the total power output. When a PWR is operational this parameter is measured and compared with predictions from a number of computer codes. For most plants these comparisons are good but in recent years, for some plants operating at high powers, this has not been the case. This AO anomaly (AOA) results from a shift in power output towards the bottom of the core as a result of a fall in the neutron flux in the upper core regions. This has a number of safety implications which could lead to a down-rating of the plant and subsequent economic losses [1].

It has been suggested that the cause of AOA is crud build up on the fuel in the top half of the core as a result of increased nucleate boiling in this region. The take-up of boron in this deposit gives increased local boron concentrations that lead to

* Corresponding author.
E-mail address: jim.henshaw@nexiasolutions.com (J. Henshaw).

0022-3115/$ - see front matter © 2006 Elsevier B.V. All rights reserved.
doi:10.1016/j.jnucmat.2005.01.028

the observed drop in the neutron flux. While it is now fairly clear that this is the mechanism for AOA, many details are not understood. Questions about the relative importance of plant operational parameters, such as boron, lithium and hydrogen concentrations in the primary water still remain, as do questions about the nature and concentration of the boron within the deposit. The temperature, pH and redox conditions within the crud are also unclear and these may have consequences for fuel performance. In order to suggest the best mitigation strategy, it is important to understand AOA further and have answers to all of these questions.

This group has investigated both crud deposition mechanisms and the chemistry taking place within the crud once it has deposited. This paper describes the work done using a relatively sophisticated model for the chemistry and physical conditions within the crud.

2. Crud chemistry model (CCM)

This section describes a chemistry model of fuel crud deposits in a PWR reactor, which treats the heat transfer, fluid flow and chemical reactions taking place in porous deposits on the fuel pins of the reactor. The model implements a realistic thermal hydraulics model together with a rigorous treatment of the thermodynamics of the high temperature aqueous solution and includes the following features:

- a Wick boiling model;
- radiolysis chemistry of water, taking into account the alpha dose from the $^{10}B(n,\alpha)^{7}Li$ reaction;
- magnetite dissolution and iron hydrolysis reactions;
- Ni–Fe ferrite dissolution and nickel hydrolysis reactions;
- Ni metal and Ni oxide formation;
- boric acid chemistry and the precipitation of lithium borate;
- non-ideal solution thermodynamics;
- the effect of solute concentration on the saturation temperature and vaporisation enthalpy of water.

The model treats the heat flux, fluid flow and chemical reactions in a deposit unit cell, consisting of one steam chimney and its surrounding porous shell. The model is one dimensional through the depth of the deposit from the bulk solution to the surface of the metal.

2.1. Thermal hydraulics

The thermal hydraulics model that is used is based on Cohen's one dimensional Wick boiling model [2]. This simulates water transport through the porous deposit and evaporation and steam transport within steam chimneys. The model is derived by considering the heat transfer in the deposit unit cell. Heat transfer is assumed to take place by conduction across the porous shell from the fuel pin towards the bulk coolant and by evaporation of steam at the surface of the chimney, as shown schematically in Fig. 1.

By considering heat balance across the cell it can be shown [2] that the temperature distribution is given by

$$\frac{d^2T}{dx^2} - \frac{2\pi r_c N_c h_e}{f k_c}(T - T_s) = 0, \tag{1}$$

where f is the fractional area of the porous shell, N_c is the area density of chimneys, r_c is the chimney radius, k_c is the thermal conductivity of the porous shell, h_e is the evaporative heat transfer coefficient and T_s is the saturation temperature (see Table 1 containing the definitions of all symbols). This equation is solved subject to the boundary conditions

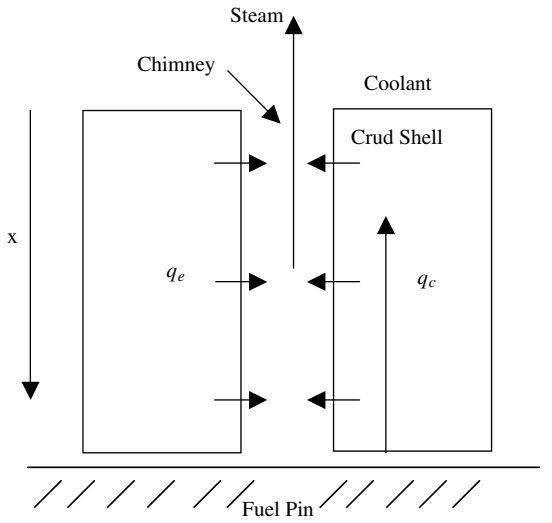

Fig. 1. Schematic diagram of heat transport during wick boiling. q_e is the evaporative heat flux and q_c the conductive heat flux.

Table 1
Definition of symbols used in text

Symbol	Definition	SI units
f	Fractional area of the porous shell	
N_c	Area density of chimneys	m^{-2}
r_c	Chimney radius	m
k_c	Thermal conductivity of the porous shell	$W\,m^{-1}\,K^{-1}$
h_e	Evaporative heat transfer coefficient	$W\,m^{-2}\,K^{-1}$
T_s	Saturation temperature	K
T_b	Bulk coolant temperature	K
Q_0	Heat flux at the surface of the fuel pin	$W\,m^{-2}$
d	Thickness of the deposit	m
H_v	Vaporisation enthalpy of water	$J\,mol^{-1}$
ρ_w	Liquid water density	$kg\,m^{-3}$
ρ_s	Steam density	$kg\,m^{-3}$
R	Gas constant	$J\,mol^{-1}\,K^{-1}$
a_w	Activity of water	
P_0	Vapour pressure of pure water	Pa
P	Vapour pressure of the solution	Pa
P_{sys}	System pressure	Pa
$\overline{V}_w^v$,	Molar volume of steam	$m^3\,mol^{-1}$
$\overline{V}_w^l$	Molar volume of liquid water	$m^3\,mol^{-1}$
μ_w^0	Chemical potential of pure water	
μ_v	Chemical potential of the vapour	
$\overline{H}$	Partial molar enthalpy	$J\,mol^{-1}$
μ	Chemical potential of the system	
H_v^0	Vaporisation enthalpy of pure water,	$J\,mol^{-1}$
ρ_w^{sat}	Density of water at the saturation temperature	$kg\,m^{-3}$
a_w	Activity of water	
m_w	Molal concentration of water	$mole\,kg^{-1}$
A	Evaporation or condensation coefficient	
M	Molecular weight of water	$g\,mol^{-1}$
ε	Porosity of the deposit	
C_l	Molar concentration in the liquid phase	$mol\,dm^{-3}$
D_l	Diffusion coefficient in the liquid within the crud	$m^2\,s^{-1}$
z	Charge number	
F	Faraday unit of charge	$C\,mol^{-1}$
ϕ'	Potential gradient	$V\,m^{-1}$
J_l	Superficial molecular flux	$mol\,m^{-2}\,s^{-1}$
D_w	Diffusion coefficient in free liquid water	$m^2\,s^{-1}$
τ	Tortuosity factor of crud	
C_b	Concentration in the bulk coolant	$mol\,dm^{-3}$
j_D	Diffusion current	$C\,m^{-2}\,s^{-1}$
σ	Effective solution conductivity	$CV^{-1}\,m^{-1}\,s^{-1}$
k_m	Mass transfer rate for species passing between the gas and liquid phases	$m\,s^{-1}$
C_v^e	Equilibrium concentration in the vapour phase	$mol\,dm^{-3}$
k_f, k_r	Forward and reverse reaction rate constants	$mol^{-1}\,dm^3\,s^{-1}$
γ	Activity coefficients	
V_s^m	Molar volume of the sth solute	$m^3\,mol^{-1}$

$$T = T_b \quad \text{at } x = 0, \tag{2a}$$

$$k_c\left(\frac{\partial T}{\partial x}\right)_{x=d} = \frac{q_0}{f} \quad \text{at } x = d, \tag{2b}$$

where T_b is the bulk coolant saturation temperature, q_0 is the heat flux at the surface of the fuel pin and d is the thickness of the deposit.

Liquid flows through the porous shell from the bulk coolant while steam is expelled through the chimney. Steady state mass conservation of water in the solution in the porous shell leads to the following equation for the liquid velocity

$$\frac{d(\rho_w u_l)}{dx} + \frac{2\pi r_c N_c}{f}\frac{h_e}{H_v}(T - T_s) = 0, \tag{3}$$

where H_v is the vaporisation enthalpy of water and ρ_w is the water density. This equation is solved subject to the boundary condition that $u_l = 0$ at $x = d$. The vapour velocity is given by

$$u_v = -\frac{f}{\pi r_c^2 N_c}\frac{\rho_w}{\rho_s}u_l, \tag{4}$$

where ρ_s is the density of steam. The thermal hydraulics model implemented in this work differs though from the simple Cohen model because T_s, H_v and h_e are all functions of the species concentrations in the water, for example the saturation temperature is obtained by solving the non-linear equation in T,

$$\ln a_w(P_0) + \frac{1}{RT}\int_{P_{sys}}^{P_0}(\overline{V}_w^v - \overline{V}_w^l)\,dP = 0, \tag{5}$$

where R, is the gas constant, a_w is the activity of water, P_0 is the vapour pressure of pure water, P the vapour pressure of the solution, P_{sys} the system pressure, and $\overline{V}_w^v$, $\overline{V}_w^l$ are the molar volumes of steam and liquid water. This equation is derived from the Clausius–Clapeyron type equation [3]

$$\left(\frac{\partial \ln a_w}{\partial P}\right)_T = \frac{\overline{V}_w^l}{RT} \tag{6}$$

and the condition that at the saturation temperature

$$\mu_w^0(P_0) = \mu_v(P_0), \tag{7}$$

where μ_w^0 is the chemical potential of pure water and μ_v the chemical potential of the vapour.

Also considering the thermodynamic relation [3]

$$\frac{\partial(\mu/T)}{\partial T} = -\frac{\overline{H}}{T^2}, \tag{8}$$

where $\overline{H}$ is the partial molar enthalpy of the solution, and μ the chemical potential of the system, leads to the following equation for the vaporisation enthalpy of the solution

$$H_v = H_v^0 - \int_{P_{sys}}^{P_0}(\overline{V}_w^v - \overline{V}_w^l)\,dP + T\int_{P_{sys}}^{P_0}\frac{\partial}{\partial T}(\overline{V}_w^v - \overline{V}_w^l)\,dP + RT^2\frac{\partial \ln a_w}{\partial T}, \tag{9}$$

where H_v^0 is the vaporisation enthalpy of pure water, obtained from the steam tables [4]. In order to solve Eqs. (5) and (9) the temperature dependence of $\overline{V}_w^l$ and $\overline{V}_w^v$ are required. In order to obtain these any direct effect that dissolved solutes may have on the density of water was neglected. This is reasonable since boric acid and its trimer, which are the most important solutes by concentration, are assumed to interact with water like water itself. Also the compressibility of water was neglected, which is reasonable because it is very small except at temperatures very close to the critical point of water. With these assumptions it is possible to write

$$\overline{V}_w^l = \frac{18.015}{\rho_w^{sat}}\ \text{cm}^3\ \text{mol}^{-1} \tag{10}$$

and

$$\overline{V}_w^v = \frac{18.015}{\rho_s}\ \text{cm}^3\ \text{mol}^{-1}, \tag{11}$$

where ρ_w^{sat} is the density of water at the saturation temperature. The temperature dependence of ρ_w^{sat} and ρ_s where obtained from Keenan and Keyes [5] and Eqs. (5) and (9) solved using Brents method [6]. This is done for a particular activity of water, a_w, which using the Gibbs–Duhem equation [3]

$$m_w\,d\ln a_w + \sum\nolimits_c m_c\,d\ln(a_w m_c) = 0 \tag{12}$$

can be expressed as

$$a_w = \frac{m_w}{m_w + \sum_c m_c}, \tag{13}$$

where m_w is the molal concentration of water, equal to 55.509 mol kg^{-1} and the sum is over molal concentrations of all species in solution.

The evaporation coefficient in Eq. (1) is given by [7]

$$h_e = \left(\frac{2A}{2-A}\right)\left(\frac{M}{2\pi R}\right)^{1/2}\frac{H_v^2}{T^{3/2}(\overline{V}_w^v - \overline{V}_w^l)}, \tag{14}$$

where A is the evaporation or condensation coefficient and M is the molecular weight of water. The thermal conductivity of the deposit, k_c, also used in Eq. (1) is calculated from Maxwell's formula [8].

It is clear therefore that the thermal hydraulics is linked to the chemistry because T_s, H_v and h_e depend on the activity of water, a_w, which in turn depends on the species concentrations in solution. In practice it is boric acid and its trimer that make the major contribution to the summation in Eq. (13).

2.2. Transport

The flow of liquid into the porous deposit at velocity u_l (given by Eq. (3)) transports dissolved boric acid and lithium hydroxide through the deposit. Also transported are hydrogen and trace

amounts of other species arising from the radiolysis of water and the dissolution of metal oxides. These species become concentrated within the porous shell where they react amongst themselves and with the oxides of the deposit. Dissolved species are transported by flow, by diffusion in their concentration gradient and, if they are charged, by drift in the electric potential gradient. For each species in the liquid phase (there is an equivalent equation for the vapour phase species, $H_2(g)$, $O_2(g)$ and $H_3BO_3(g)$) it is possible to write

$$\frac{\partial C_l}{\partial t} = \left(\frac{\partial C_l}{\partial t}\right)_R + \left(\frac{\partial C_l}{\partial t}\right)_P - \frac{1}{\varepsilon}\frac{\partial J_l}{\partial x}, \tag{15}$$

where C_l is the concentration in the liquid, and the first term on the right of the equation is due to changing species concentrations by chemical reaction (subscript R for reaction), the second term is due to liquid/steam partitioning (subscript P for partitioning) and the third term is due to transport. ε is the porosity of the deposit, which is the fraction of free space present per unit volume of crud.

The superficial molecular flux J_l in Eq. (15) is given by [9]

$$J_l = -D_l\frac{\partial C_l}{\partial x} - \frac{zFD_l}{RT}\phi' C_l + u_l C_l, \tag{16}$$

where D_l is the diffusion coefficient, z is the charge number, F is the Faraday unit of charge, and ϕ' is the potential gradient. To simplify the notation, subscripts are not appended to J_l, C_l, D_l and z to differentiate the species. The diffusion coefficient D_l in the porous shell is related to the diffusion coefficient in liquid water D_w by the following empirical equation

$$D_l = \frac{\varepsilon D_w}{\tau}, \tag{17}$$

where τ is the tortuosity factor of the crud, representing an effective path length through the deposit and is defined by Eq. (17). Eq. (15) is solved subject to the boundary condition that $C_l = C_b$ at $x = 0$, where C_b is the concentration in the bulk coolant.

The potential gradient in Eq. (15) is obtained from a generalised Ohm's law equation [9]

$$\sigma\phi' = -j_D, \tag{18}$$

where j_D is the diffusion current [9] and σ the effective solution conductivity.

The model treats the partitioning of three volatile species, boric acid, hydrogen and radiolytically produced oxygen, from the liquid phase in the porous shell into the vapour phase in the chimney. The rate of loss of these species is given by

$$\left(\frac{\partial C_l}{\partial t}\right)_P = -\frac{2\pi r_c N_c}{\varepsilon f}k_m(C_v^e - C_v), \tag{19}$$

where k_m is the mass transfer rate for species passing between the gas and liquid phases and C_v^e is the equilibrium concentration in the vapour phase, determined by the relevant partitioning constant [10].

2.3. Chemistry

Chemical reactions are included in CCM in the form of rate equations, which express the rate of change of species concentrations as equal to the product of a rate constant and the concentrations of the reactant concentrations. The term $\left(\frac{\partial C_l}{\partial t}\right)_R$ in Eq. (15) is then the net rate of change of the species concentration due to all the relevant reactions in the system. Many of the reactions included in the model are treated as equilibria with rate equations used to express both the forward and reverse reactions. In these cases the reverse rate constant is calculated knowing the forward rate and equilibrium constant. For example for the reaction

$$A + B = C. \tag{20}$$

The equation describing the rate of change of [A] would be

$$\frac{dc_A}{dt} = -k_f c_A c_B + k_r c_C, \tag{21}$$

where k_f is the forward rate and k_r is the reverse reaction rate constant. The thermodynamic equilibrium constant for the reaction is related to the ratio of these constants. At equilibrium in the steady state, $dc_A/dt = 0$ and the ratio of the forward and reverse rate constants is given by

$$\frac{k_f}{k_r} = \frac{c_C}{c_A c_B}, \tag{22}$$

where the c are now equilibrium *molar* concentrations. The thermodynamic equilibrium expression for this reaction is given by

$$K = \frac{m_C}{m_A m_B}\frac{\gamma_C}{\gamma_A\gamma_B}, \tag{23}$$

where the m are *molal* concentrations and the γ are activity coefficients. Converting the molal concentrations to molar concentrations leads to the

following expression for the ratio of the forward and reverse rate constants

$$\frac{k_f}{k_r} = \frac{K}{\zeta \rho_w} \frac{\gamma_A \gamma_B}{\gamma_C}, \tag{24}$$

where

$$\zeta = 1 - \sum m_s V_s^m. \tag{25}$$

V_s^m is the molar volume of the sth solute and the sum is over all dissolved species. The activity coefficients γ are calculated here using the Meissner equations [10]. These non-ideal corrections are necessary because solution concentrations within the deposit can be large, of the order of several molar. Of the parameters on the right hand side of Eq. (24), K and ρ_w are functions of temperature, ζ is a function of concentration, and the γ's are functions of both temperature and concentration.

The different types of chemical reactions included in the model are summarised below, together with some examples of each and the sources for the rate and equilibrium data.

(1) The ionisation of water

$$H_2O \rightleftharpoons H^+ + OH^- \tag{26}$$

The equilibrium constant for this reaction is calculated using the correlation of Marshall and Franck [11], taken from the chapter by Lindsay in the ASME Handbook on Water technology [10].

(2) Metal ion hydrolysis reactions [10,12–14]

$$Ni^{2+} + 2Fe^{2+} + 4H_2O \rightleftharpoons NiFe_2O_4(s) + 6H^+ + H_2(aq) \tag{27}$$

$$Ni^{2+} + H_2O \rightleftharpoons NiOH^+ + H^+ \tag{28}$$

(3) Boric acid equilibria

$$B(OH)_3 + OH^- \rightleftharpoons B(OH)_4^- \tag{29}$$

$$2B(OH)_3 + OH^- \rightleftharpoons B_2O(OH)_5^- + H_2O \tag{30}$$

$$3B(OH)_3 \rightleftharpoons B_3O_3(OH)_3 + 3H_2O \tag{31}$$

Equilibrium constants for these reactions are based on an experimental study of Weres [15] and the work of Byers et al. [16].

(4) Precipitation and dissolution reactions

$$LiBO_2(s) + H_2O + H^+ \rightleftharpoons Li^+ + B(OH)_3 \tag{32}$$

The equilibrium constants for this reaction are taken from the experimental study of Byers et al. [16] for the dissolution of lithium borate.

(5) Liquid to vapour partitioning reactions [10]

$$H_2(l) \rightleftharpoons H_2(v) \tag{33}$$

$$B(OH)_3(l) \rightleftharpoons B(OH)_3(v) \tag{34}$$

(6) Radiolysis chemistry of water

Neutron, gamma and alpha radiation interacts with water causing it to decompose to the radical products e^-, H^+, H, and OH and the molecular products H_2 and H_2O_2. Gamma radiation gives largely radical species, while alpha and neutron radiation give largely molecular species. The yields for the different species are expressed through the G-values, which determine the number of molecules produced per 100 eV of radiation energy absorbed. The G-values for these reactions where taken from Elliot et al. [17].

The primary radiolytic species undergo a series of chemical reactions, for example

$$H + H_2O = H_2 + OH \tag{35}$$

$$e^- + H_2O_2 = OH^- + OH \tag{36}$$

$$H + H_2O_2 = OH + H_2O \tag{37}$$

$$OH + H_2O_2 = H_2O + HO_2 \tag{38}$$

$$OH + H_2 = H_2O + H \tag{39}$$

In total there are forty radiolysis reactions in the model. The rate constants for use in high temperature water come from the report by Elliot et al. [17].

All the equations were implemented and solved using the numerical integration program FACSIMILE [18], which uses a form of Gears method for solving stiff differential equations. The following Section discusses some of the results obtained with the model.

3. Discussion of CCM results

Before discussing the results of the model it is important to understand the aims of its development. The model was developed to explain a number of observations that have been made concerning AOA. These observations are stated here [1].

- AOA is first observed in plants where crud deposits are believed to have built up to ~20–30 μm.
- In some very thick crud deposits (>80 μm) the boron mineral bonaccordite (Ni_2FeBO_5) has been identified. This indicates fairly extreme conditions within the crud [19].

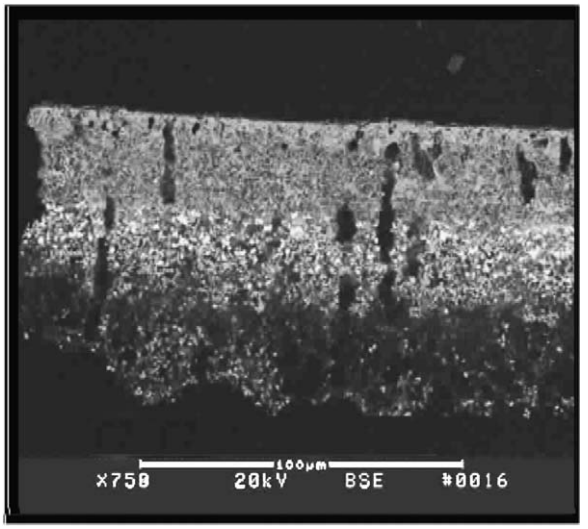

Fig. 2. A thick crud flake showing three distinct layers. The middle white zone contains ZrO_2.

- A few plants with thick deposits have seen a layer of ZrO_2 material some distance above the fuel clad oxide surface, see Fig. 2.
- Examination of fuel crud scrapes indicate a Ni rich deposit compared to crud scrapes from non-AOA plants.
- Thick crud contains relatively less chromium than thin crud.

Calculations have been performed using CCM over a wide range of operating conditions, the standard input conditions being those outlined in Table 2. These are representative PWR conditions.

Fig. 3 shows how the Li^+, Boric acid and $LiBO_2$(s) concentrations vary through a 59 μm thick crud deposit for typical PWR conditions. The results indicate the boric acid concentration is approximately 2 M near the fuel surface (a concentration factor of 25 compared to the bulk). Also important in the liquid phase is the Boric acid trimer, which contains approximately 2 M Boron near the fuel surface. The Li^+ ion concentration rises to 0.01 M (a concentration factor of 54). What is interesting about these results is that $LiBO_2$(s) precipitates out at a depth of 35–40 μm. This is near the crud thickness, based on scrape measurements, where AOA starts to be observed [1]. It should be noted that nothing in the model was adjusted to give this result and it is simply a consequence of the physics and chemistry that have been implemented.

Table 2
Standard PWR input conditions for the CCM model

Parameter	Value
Coolant saturation temperature/°C	345
System pressure/atm	153
Chimney density/mm^2	3000
Chimney radius/μm	2.5
Porosity	0.8
Tortuosity	2.5
Deposit depth/μm	25–60
Heat flux W/m^{-2}	10^6
Li/ppm	2
B/ppm	1200
H_2/cc (STP) kg^{-1}	25
γ Dose rate/Mrad h^{-1}	1200
n Dose rate/Mrad h^{-1}	2400
n Flux/cm^{-2} s^{-1}	3.6×10^{14}

Previous modelling results by other groups had indicated that $LiBO_2$(s) would not precipitate out until crud thicknesses reached well above a hundred microns [20]. The reason this model predicts precipitation at much smaller crud thicknesses can be understood from Fig. 4, which shows how the temperature varies through the crud for a 35 and 59 μm thick deposit. Fig. 4 indicates the rise in species concentrations towards the bottom of the crud causes a rise in the saturation temperature and because the solubility of $LiBO_2$(s) falls with increasing temperature it precipitates. This rise in temperature was not accounted for in previous models [20].

For the 59 μm thick crud the rise in temperature is dramatic, reaching temperatures near 400 °C, well above the critical point for pure water (approximately 374 °C). Part of the reason for this rise is the fact that as the temperature increases the enthalpy of vaporisation decreases (it is zero at the critical point temperature). This means that less energy is removed by evaporation into the chimney (at the critical point temperature no energy removal occurs by evaporation). The shutting down of evaporation therefore causes the temperature to rise even further. Extreme conditions may therefore exist at the bottom of thick crud and may explain the formation of the mineral bonaccordite [1]. The work of Sawicki indicates temperatures just above 400 °C may be required to form this mineral [19]. The potential effect of reaching near 400 °C on cladding corrosion in the model has not been reconciled yet.

Fig. 5 shows the variation in pH_T through the porous deposit for a 35 and 59 μm thick deposit. For the 35 μm thick deposit the pH falls through the deposit from the water side to the fuel side. The pH for the 59 μm thick deposit shows a

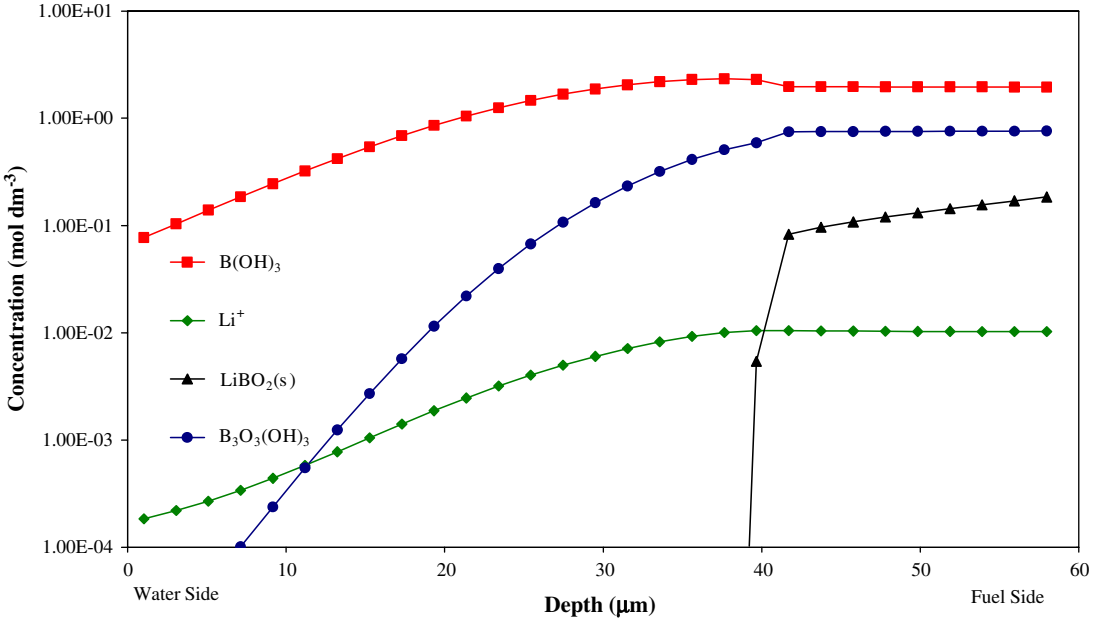

Fig. 3. Li^+, Boric acid concentration and amount of $LiBO_2$(s) against depth for a 59 μm thick deposit. Calculation with 2 ppm Li, 1200 ppm B and 25 cm^3 kg^{-1} (STP) H_2.

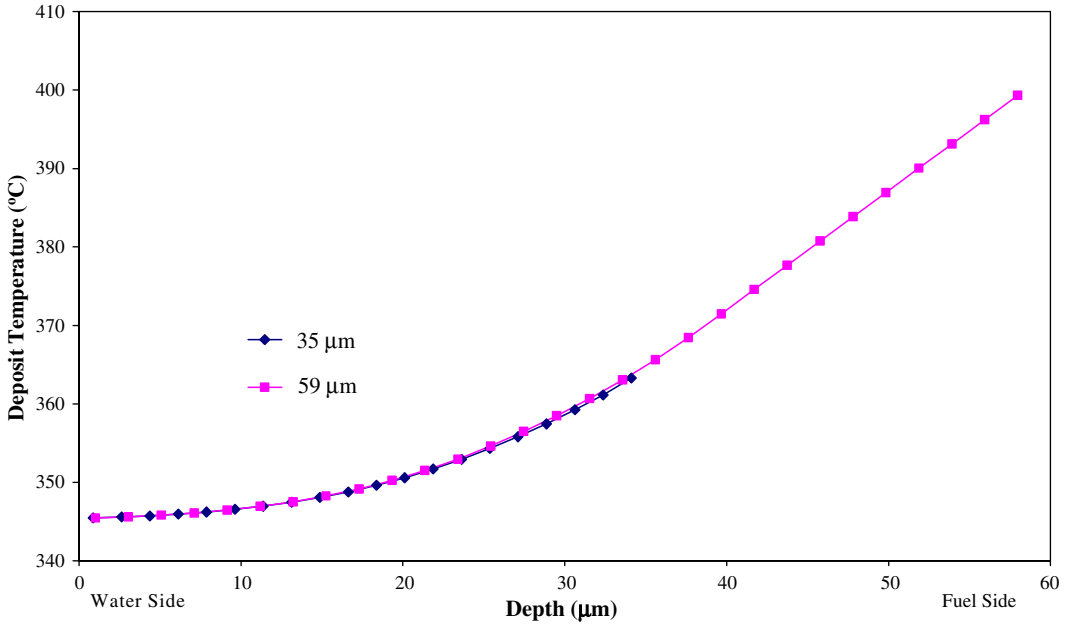

Fig. 4. Temperature across the deposit for a 35 and 59 μm thick deposit. Calculation with 2 ppm Li, 1200 ppm B and 25 cm^3 kg^{-1} (STP) H_2.

complicated behaviour with a relatively steady pH near the fuel surface followed by a sudden fall in pH and then rising again towards the water side of the crud. The steady pH near the fuel pin surface is due to the presence of $LiBO_2$(s) which buffers the pH in this region. If $LiBO_2$(s) was not allowed to precipitate out in the model the pH in this region would be very large (9–10). For the thick deposit, since ZrO_2 solubility tends to rise with increasing pH, its solubility is likely to be larger nearer the fuel

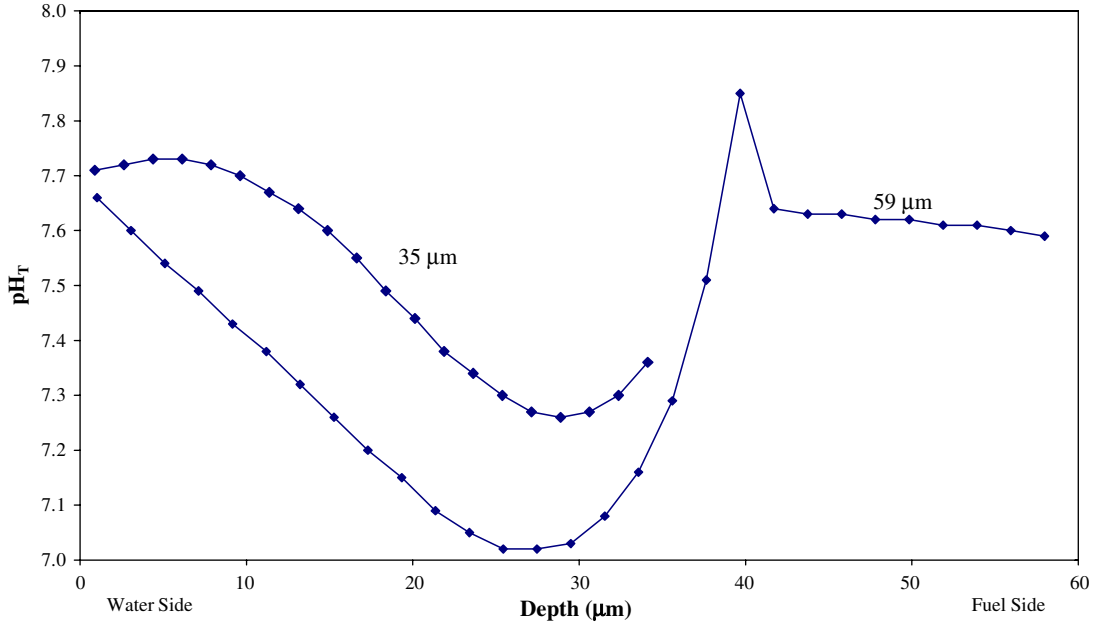

Fig. 5. pH at temperature across the deposit for 35 and 59 μm thick deposits. Calculation with 2 ppm Li, 1200 ppm B and 25 cm^3 kg^{-1} (STP) H_2.

pin surface than at 20 μm away from the surface. The sharp fall in pH away from the fuel pin surface may give rise to ZrO_2 precipitation at this point, providing an explanation for the band of this oxide seen in some thick deposits, but not in thin deposits. The high temperature and high Lithium ion concentration near the fuel surface would also facilitate Zr-oxide dissolution in this region.

A further issue which the model was developed to resolve is the relative amounts of Ni and Fe within the deposit and the fact that these tend to be Ni rich in thick deposits. Suffice to say that the model, as yet, has not provided a credible explanation for this observation. This is because the issue is complicated by several different factors:

1. The form of Ni and Fe depositing on the fuel pin from the bulk solution.
2. The rate of inter-conversion of the various mineral forms.
3. The pH conditions that exist within the crud.
4. The redox conditions within the crud.
5. The temperature within the crud.

The situation is complicated further by the fact that redox conditions, pH and temperature will change during the fuel cycle. This can be seen in Fig. 6 which shows how the temperature at the bottom of the crud deposit changes with crud thickness and bulk water boron concentration. For a 59 μm thick deposit the temperature at the bottom of the deposit falls by 20 °C as the boron concentration falls from 1800 ppm to 300 ppm.

Fig. 7 shows the calculated hydrogen peroxide concentration at the bottom of the deposit as a function of crud thickness for different bulk water boron concentrations. It is clear from Fig. 7 that the redox conditions could be relatively oxidising at the bottom of thick crud deposits. Peroxide concentrations rise to several hundred ppb, compared to typical bulk water concentrations of less than 1 ppb. This is because the chimney through which steam is passing strips hydrogen out of the adjacent water. The process is analogous to a boiling fuel channel in a Boiling Water Reactor but on a micro scale. The variation in peroxide with bulk water boron concentration is interesting, at 1200 and 1800 ppm B, the peroxide concentration at the base of the 60 μm deposit is approximately 16–17 ppb. Decreasing the boron to 600 ppm causes the peroxide to rise rapidly to 350 ppb, while decreasing the boron further to 300 ppm causes the peroxide to fall to approximately 100 ppb. Increasing the boron concentration increases the alpha particle dose rate in the model and, since alpha particles give high yields of molecular products such as H_2O_2, this

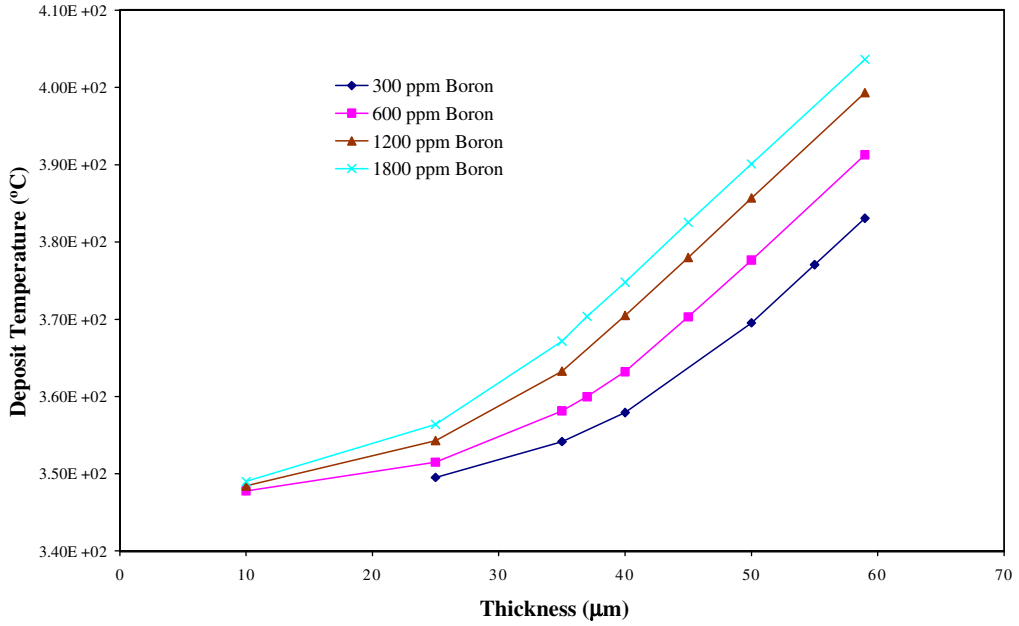

Fig. 6. Temperature at the bottom of the crud for different crud thicknesses, at different bulk water boron concentrations.

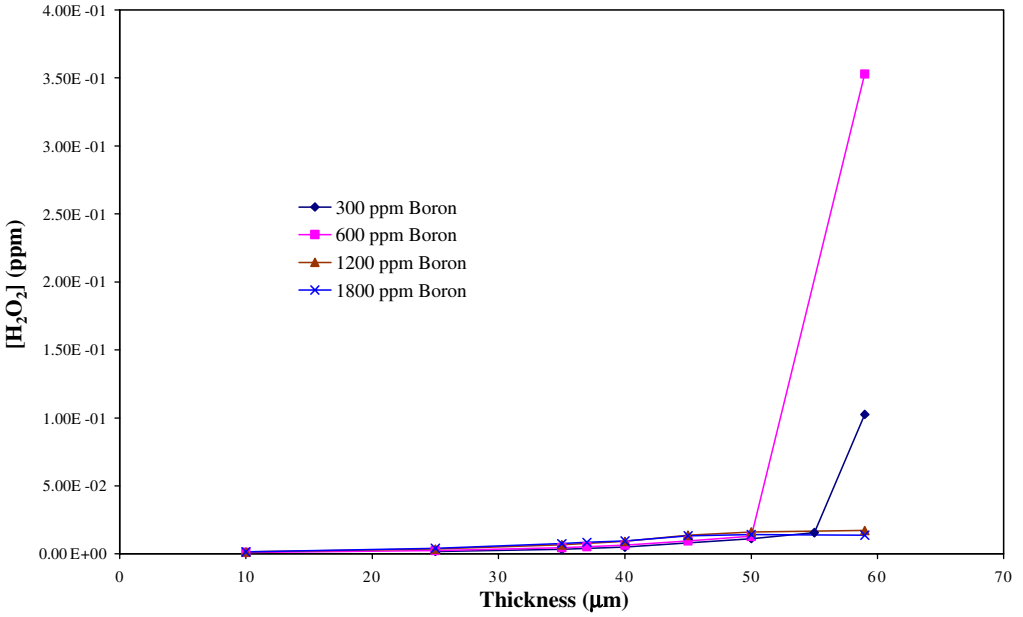

Fig. 7. Hydrogen peroxide concentrations at the bottom of the crud for different crud thicknesses, at different bulk water boron concentrations.

increases the peroxide concentration. However, at say 300 ppm B, less of the crud will be above the critical temperature of water than for a 1800 ppm B solution. This means that evaporative heat loss will take place into the wick chimney over a longer region at 300 ppm B compared to 1800 ppm B. In which case partitioning of H_2 into the steam phase occurs more at 300 ppm B compared to higher boron concentrations. Therefore we have two opposing effects of decreasing boron; on the one hand it lowers the alpha dose and therefore decreases the peroxide yield, but on the other hand

it lowers the hydrogen concentrations within the liquid present in the deposit, increasing the peroxide concentration. In addition the solubility of H_2 will be lower at low boron because of the reduced temperature at the base of the deposit. Which of these processes dominate determines whether significant peroxide is produced. The observation that thick crud is depleted in chromium supports the existence of oxidising conditions in the crud. This is because chromium solubility increases with increasing oxidising conditions and so is more likely to leach out of thick crud deposits.

These variations in pH, redox conditions and temperature over a cycle will influence the crud composition and further work is planned to understand this behaviour.

4. Summary

The model that has been presented here is a 1-dimensional Wick boiling model in which the thermal hydraulics is coupled with the chemistry. All the chemistry that is relevant to crud deposits on fuel pins is considered, including the radiolysis chemistry of water. The model provides credible explanations for many of the observed fuel crud/AOA phenomena, such as the onset of AOA at crud thicknesses above 35 μm, the presence of bonaccordite in only thick deposits, the presence of ZrO_2 layers in thick crud and chromium depletion in thick deposits. Further work is being carried out to try and understand the composition of the crud and in particular the relative amounts of Ni and Fe present.

Acknowledgements

This work was funded by the UK's Health and Safety Executive, British Energy and EPRI. Thanks also go to Keith Garbett (Consultant to British Energy) and Art Byers, Dave Chapman (Westinghouse).

References

[1] (a) P. Frattini, E. Blandford, D. Hussey, A. Morvan, J. Blok, E. Decossin, N. Faner, Modelling axial offset anomaly, paper 7.1, in: Proceedings of the International Conference on Water Chemistry of Nuclear Reactor Systems, SanFrancisco, October 2004;
(b) A. Byers, J. Deshon, Structure and chemistry of PWR CRUD, paper 7.5, in: Proceedings of the International Conference on Water Chemistry of Nuclear Reactor Systems, SanFrancisco, October 2004.
[2] P. Cohen, AIChE Symp. Ser. 70 (138) (1974) 71.
[3] W.J. Moore, Physical Chemistry, 5th Ed., Longman Group Ltd., 1972.
[4] F.D. Hamblin, Abridged Thermodynamic and Thermochemical Tables, Pergamon, Oxford, 1971.
[5] J.H. Keenan, F.G. Keyes, Thermodynamic Properties of Steam, 1st Ed., Wiley, New York, 1936.
[6] W.H. Press, S.A. Teukolsky, W.T. Vetterling, B.P. Flannery, Numerical Recipes in C, 2nd Ed., Cambridge University, 1992.
[7] C. Pan, B.G. Jones, A.J. Michiels, Wick boiling performance in porous deposits with chimneys, in: ASME/AIChE/ANS National Heat Transfer Symposium on Multiphase Flow and Heat Transfer, Denver, August 1985.
[8] A.C. Smith, Fluid Flow, heat and mass transfer, in: Paul Cohen (Ed.), The ASME Handbook on Water Technology for Thermal Power Systems, ASME, New York, 1989.
[9] J. Henshaw, J.C. McGurk, A model of radiation chemistry effects on crack corrosion, in: Proceedings of the 7th International Conference on Water Chemistry of Nuclear Reactor Systems, Bournemouth 1996, vol. 2, p. 513.
[10] W.T. Lindsay Jr., Chemistry of steam cycle solutions: principles, in: Paul Cohen (Ed.), The ASME Handbook on Water Technology for Thermal Power Systems, ASME, New York, 1989.
[11] W.L. Marshall, E.U. Franck, J. Chem. Ref. Data 10 (1981) 295.
[12] F.H. Sweeton, C.F. Baes Jr., J. Chem. Thermodyn. 2 (1970) 479.
[13] P.R. Tremaine, J.C. LeBlanc, J. Solut. Chem. 9 (1980) 415.
[14] I. Lambert, J. LeCompte, P. Beslu, F. Joyer, Corrosion product solubility in PWR primary coolant, in: Proceedings of 4th Conference on Water Chemistry of Nuclear Reactor Systems, BNES Bournemouth, 1986.
[15] O. Weres, J. Solut. Chem. 24 (1995) 409.
[16] W.A. Byers, W.T. Lindsay Jr., R.H. Kunig, J. Solut. Chem. 29 (2000) 541.
[17] (a) A.J. Elliot, D.R. McCracken, G.V. Buxton, N.D. Wood, J. Chem. Soc. Faraday Trans. 86 (1990) 1539;
(b) A.J. Elliot, AECL-11073, COG-94-167, 1994.
[18] Facsimile, a numerical integration package, sold by MCPA Software Ltd. Available from: <www-mcpa-software.com>.
[19] J.A. Sawicki, Nuclear chemistry model of borated fuel crud, in: Proceedings of the International Conference on Water Chemistry of Nuclear Reactor Systems, Avignon, April 2002.
[20] P.L. Frattini, J. Blok, S. Chauffriat, J. Sawicki, J. Riddle, Axial offset anomaly: coupling of PWR primary chemistry with core design, in: Proceedings of the 8th International Conference on Water Chemistry of Nuclear Reactor Systems, vol. 1, p. 24, Bournemouth, October 2000.